
**Journal of Sulfur Chemistry**
Publication details, including instructions for authors and subscription information:
http://www.informaworld.com/smpp/title~content=t713926081

# Spectroscopic and biological studies of mono- or binuclear complexes derived from thio-Schiff bases of some transition metals

Azza A. A. Abou-Hussein[a]
[a] Department of Chemistry, Women Faculty of Arts, Science and Education, Ain Shams University, Cairo, Egypt

Online publication date: 28 September 2010

**To cite this Article** Abou-Hussein, Azza A. A.(2010) 'Spectroscopic and biological studies of mono- or binuclear complexes derived from thio-Schiff bases of some transition metals', Journal of Sulfur Chemistry, 31: 5, 427 — 446
**To link to this Article: DOI:** 10.1080/17415993.2010.503774
**URL:** http://dx.doi.org/10.1080/17415993.2010.503774

*Journal of Sulfur Chemistry*
Vol. 31, No. 5, October 2010, 427–446

Taylor & Francis
Taylor & Francis Group

# Spectroscopic and biological studies of mono- or binuclear complexes derived from thio-Schiff bases of some transition metals

Azza A.A. Abou-Hussein*

*Department of Chemistry, Women Faculty of Arts, Science and Education, Ain Shams University, Cairo, Egypt*

(*Received 25 February 2010; final version received 20 June 2010*)



Two novel Schiff base ligands, 4,6-bis((*E*)-1-(2-mercaptophenylimino)ethyl)benzene-1,3-diol, $H_4L_a$, and 1,2-((*E*)-1-(6-((*E*)-1-(2-mercaptophenylimino)ethyl)pyridine-2-yl)ethylideneamino)benzenthiol, $H_2L_b$, have been synthesized by the condensation of 4,6-diacetyl resorcinol (DAR) or 2,6-diacetyl pyridine (DAP) with 2-aminobenzenthiol (ABT), in the molar ratio 1:2 [1 (DAR or DAP):2 ABT]. The structures of ligands were elucidated by elemental analysis, infrared (IR), UV–VIS as well as $^1$H-NMR. Reaction of the Schiff base ligands with the transition metals Co(II), Ni(II), Cu(II), Zn(II), VO(IV) and Ru(III) afforded two series of the corresponding transition metal complexes in the molar ratio 1:2 or 1:1. The ligand, $H_4L_a$, behaves as tetrabasic hexadentate, which hosts the two metal ions at the centers of two SNO sites, while $H_2L_b$ acts as a compartmental dibasic pentadentate ligand forming mono- or binuclear complexes through the coordinate sites $N_3S_2$. The structures of the newly prepared complexes were characterized on the basis of the elemental analysis, spectroscopic data (IR, UV–VIS, $^1$H-NMR and ESR spectra along with magnetic susceptibility measurements) besides the molar conductance measurements and thermal gravimetric analyses. The bonding sites are the azomethane, sulfur atoms and phenolic oxygen for $H_4L_a$ or pyridine nitrogen for $H_2L_b$. The complexes exhibit mono- or binuclear structures, distorted octahedral, tetrahedral, square planar or square pyramid structure. Synthesized compounds have also been screened for their biological activity against species of pathogenic fungi and bacteria and were found to possess appreciable fungicidal and bactericidal properties.

**Keywords:** thio-Schiff base ligands; transition metal complexes; spectroscopy; biological activates

## 1. Introduction

Over the past few years, thio-Schiff bases and their metal complexes have received considerable attention in the field of coordination chemistry (*1–4*). Molecules containing electron-acceptor Schiff bases are of great interest because of their potential therapeutic and pharmacological properties (*5–7*) and because of their ability to serve as polymeric ultraviolet stabilizers (*8*). It has been reported that some of these complexes have increased activity when administrated as metal complexes (*9*) and their interactions with DNA have been reported (*10, 11*). Moreover, it is well

*Email: azza_aly2000@yahoo.com

ISSN 1741-5993 print/ISSN 1741-6000 online

DOI: 10.1080/17415993.2010.503774
http://www.informaworld.com

known that Schiff base complexes have the ability to bind reversibly $O_2$ and $CO_2$ (*12*). Their potential catalytic behavior for electrochemical reduction of organic halides, hydrogenation in metallo-enzyme (*13*, *14*) and recovering of metals from an aqua phase by solvent extractions have been reported (*15*, *16*). In the present work, two series of mono- or binuclear complexes have been synthesized and characterized from the newly synthesized thio-Schiff bases, $H_4L_a$, 4,6-bis((*E*)-1-(2-mercaptophenylimino)ethyl)benzene-1,3-diol and $H_2L_b$ (1,2-((*E*)-1-(6-((*E*)-1-(2-mercaptophenylimino)ethyl)pyridine-2-yl)-ethylideneamino)benzenthiol. We report here the preparation and magnetic, spectroscopic characterization of two series of transition metal complexes of Co(II), Ni(II), Cu(II), Zn(II), VO(IV) and Ru(III). $^1$H-NMR spectra, various ligand field parameters, (10 Dq, $B$ and $\beta$ were calculated) and ESR spectra as well as thermal gravimetric analyses (TGAs) have also been studied for some selected metal complexes.

*In vitro* biological screening of the synthesized ligands and complexes were carried out against the phytopathogenic bacteria (*Azotobacter* and *Rhizobium*) and fungi (*Aspergillus niger* and *Fusarium oxysporium*). It has been observed that the antimicrobial activities of metal complexes are higher than the free ligands.



## 2. Results and discussion

Schiff bases $H_4L_a$ and $H_2L_b$ were synthesized by the condensation of the bicarboxyl compounds 4,6-diacetyl resorcinol (DAR) or 2,6-diacetyl pyridine (DAP) with 2-aminobenzenthiol (ABT) in the molar ratio 1:2 (1 DAR or DAP:2 ABT) (Schemes 1 and 2). The structures of the thio-Schiff bases are identified by elemental analysis, infrared (IR), UV–VIS and $^1$H-NMR. The physical and analytical data of the ligands and their corresponding transition metal complexes are listed in Table 1. The mode of binding of both thio-Schiff base ligands to the metal ions was elucidated by recording the IR spectra of the complexes and comparing it with the spectra of the free ligands. The IR frequencies of the Schiff bases $H_4L_a$ and $H_2L_b$ and their assignments are listed in Table 2.

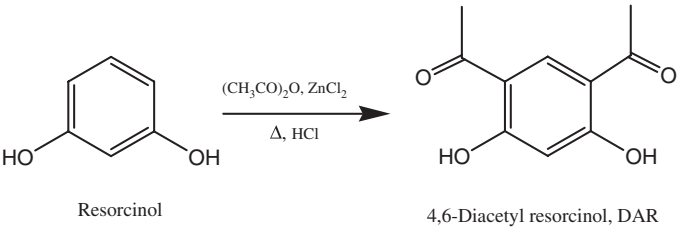


Resorcinol — 4,6-Diacetyl resorcinol, DAR

Scheme 1. Synthetic preparation of 2,6-diacetyl resorcinol, DAR.

### 2.1. *IR spectra*

The IR spectra of the thio-Schiff bases $H_4L_a$ and $H_2L_b$ exhibited strong sharp bands at 3216 and 3244 cm$^{-1}$, respectively, due to the stretching vibrations of the intermolecular hydrogen bonded N $\cdots$ HS or OH $\cdots$ N $\cdots$ HS (*17*, *18*). $H_4L_a$ spectra show a medium broad band in the region 3050–3300 cm$^{-1}$ and another weak band at 2560 cm$^{-1}$, assigned to the $-$OH and $-$SH groups, respectively (*19*). The disappearance of these two bands on complexation indicates the deprotonation of the hydrogen of the phenolic oxygen and thiol groups upon coordination with the metal ions (*20*). Similar behavior has been observed for the Schiff base $H_2L_b$, where the band assigned to the stretching vibration of the thiol group (ca. 2523 cm$^{-1}$) also disappeared

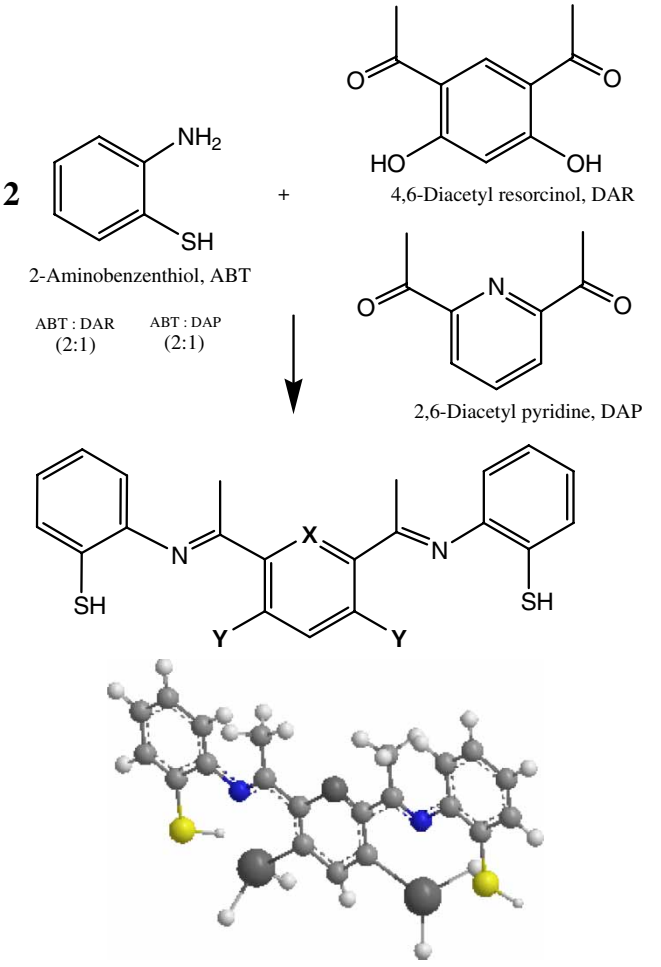


For $H_4L_a$, X=C and Y=OH, while $H_2L_a$ X=N and Y=H

Scheme 2. Synthetic preparation of the Schiff base $H_4L_a$ and $H_2L_b$ ligands.

due to the fact that coordination takes place through sulfur atoms after deprotonation (*21*). One of the most conceptual features of the IR spectra of the Schiff bases is the disappearance of the characteristic carbonyl group $\nu$(C=O) bands in both DAR and DAP as a result of the condensation and the appearance of new intense bands at 1638 and 1642 $cm^{-1}$ for the $H_4L_a$ and $H_2L_b$ Schiff bases, respectively, which are assigned to the mixed mode of vibration arising from azomethine moiety, $\nu$(C=N) and $\nu$(C=C) vibration (*22*). On complexation, these bands were shifted to lower frequencies around 1616–1578 $cm^{-1}$, for all the complexes of thio-Schiff bases, indicating the coordination through the nitrogen atoms of the azomethine groups (*23*, *24*). Conclusive evidence of the bonding is also shown by the observation of new bands in the spectra of metal complexes which appeared with a medium or weak intensity at the region 467–435 $cm^{-1}$ due to $\nu$(M−N) stretching vibrations (*25*). The bands at 1126 and 1145 $cm^{-1}$, assigned to the $\nu$(N−N) absorption, were shifted to 1135 and 1157 $cm^{-1}$ for $H_4L_a$ and $H_2L_b$, respectively, supporting the involvement of nitrogen atom of the azomethine group via coordination (*26*). These observations are inconsistent with the appearance of new weak to medium bands in the two regions 543–573 and 356–382 $cm^{-1}$, which could be assigned to the stretching frequencies of $\nu$(M−O) and $\nu$(M−S) bands, respectively,

confirming that the chelation to the metal ions is achieved by phenolic oxygen and thiol-sulfur atoms (*27*). It is worth mentioning that the vibration band at 990 $cm^{-1}$, corresponding to the ring breathing mode of pyridine nitrogen disappeared in all the complexes of thio-Schiff base $H_2L_b$ and a new medium-intensity band is observed in the range 1008–1028 $cm^{-1}$, as a result of the contribution of the pyridine nitrogen to the metal ion (*28*). One of the most fundamental features of the spectra of some complexes is the appearance of a broad band between the range 3300 and 3500 $cm^{-1}$, which could be assigned to the stretching frequencies of the hydroxyl group of either the crystalline or the coordinated water molecules associated with the complex (*29*). This result is also confirmed by the elemental analysis as well as by TGA for some selected complexes. It is worth mentioning that the absorptions at 324 and 332 $cm^{-1}$ in the spectra of Ru(III) complexes (**6**) and (**12**) were attributed to $\nu$(Ru−Cl) vibrations (*30*). In addition, for green vanadyl complexes, a strong band is observed at 970 and 990 $cm^{-1}$, which is assigned to the stretching vibrations of $\nu$(V=O) band of (**5**) and (**11**) complexes, respectively.

The $NO_3^-$ ions are coordinated to the metal center as unidentate ligands for both complexes $[Co_2(L_b)(H_2O)_5(NO_3)_2]\cdot H_2O$ (**7**) and $[Ni_2(L_b)(H_2O)_3(NO_3)_2]\cdot 2H_2O$ (**8**) with a $C_{2v}$ symmetry. Each unidentate nitrate group possesses three non-degenerated modes of vibrations ($\nu_s$, $\nu_{s'}$ and $\nu_{as}$), which appeared at 1374–1452, 1323–1376 and 778–823 $cm^{-1}$, respectively, for the metal complexes that contain the nitrate groups. The $\nu_s(NO_3^-)$ of the unidentate $NO_3^-$ is markedly shifted to lower frequencies compared with that of the free nitrate (1700–1800 $cm^{-1}$). This could be a factor measuring the covalent bond strength which is formed due to the transfer of electron density from $NO_3^-$ to the metal ion (*27*).



### 2.2. *Electronic spectra*

The electronic spectra of the thio-Schiff base ligands $H_4L_a$ and $H_2L_b$ show mainly four absorption bands at 228, 297, 322 and 372 nm for the former ligand and 251, 268, 323 and 356 nm for the latter one. The two bands at higher energy arises from $\pi$–$\pi^*$ transitions of the phenyl rings ($^1L_a \rightarrow {}^1L_b$) and ($^1L_b \rightarrow {}^1A_1$). On the other hand, the bands appearing at the lower energy side is attributed to the $\pi$–$\pi^*$ transition associated with the azomethine chromospheres. The last broad band at 410–412 nm is due to the n $\rightarrow \pi^*$ transition which is overlapping with the intermolecular CT from the phenyl ring to the azomethine group (*31*). On complexation, the absorption bands are shifted to lower wavenumbers compared with the free ligands as a result of coordination via the nitrogen atoms of the azomethine groups. The d–d transitions of the metal complexes have lower value than the transition bands of the ligands (Table 3). The bands located around 230–380 and at 390 nm were assigned to $\pi$–$\pi^*$ transitions within the aromatic rings in the ligands while the absorption band in the range 325–345 nm could be assigned to C=N group, and on the other hand, the bands observed at 400–465 nm could be assigned to the charge transfer transition (*32*).

The electronic spectra of $[Co_2(L_a)(H_2O)_2]$ complex (**1**) showed a broad band at 534 nm which is consistent with $^2A_{1g} \leftarrow {}^2B_{2g}$ corresponding to a square planar geometry. The magnetic moment of the complex is in agreement with the presence of one unpaired electron (1.87 $\mu_B$) in a square planar structure (*33*). On the other hand, the electronic spectrum of $[Co_2(L_b)(H_2O)_5(NO_3)_2]\cdot H_2O$ complex (**7**) showed that the complex may be proposed as distorted octahedral structures, based on the appearance of absorption bands at 665 and 558 nm which are normally assigned to $^4A_{2g}(F) \leftarrow {}^4T_{1g}(F)$ and $^4T_{1g}(P) \leftarrow {}^4T_{1g}(F)$ transitions. The spectra of Co(II) octahedral complexes usually consist of three bands. The third expected band which is due to $^4T_{2g}(F) \leftarrow {}^4T_{1g}(F)$ transition was not observed due to the limitations in the scanning range of the instrument used. The measured magnetic moment is 5.14 $\mu_B$ which provides complementary means with the formation of a high-spin octahedral geometry and lies in the range reported for the octahedral structure (*34*). The ligand field parameters such as Racah inter-electronic repulsion parameter ($B'$), covalency factor

Table 1. Physicochemical properties of the Schiff base ligands $H_4L_a$ and $H_2L_b$ and their transition metal complexes.

| Ligand/complex | | MF | M Wt. | Yield (%) | Color | DP (°C) | Elemental analyses, Calc./(Found) (%) | | | |
|---|---|---|---|---|---|---|---|---|---|---|
| | | | | | | | %C | %H | %N | %M |
| **I** | $H_4L_a$ | $C_{22}H_{20}N_2O_2S_2$ | 408.54 | 68.71 | Cream | 182 | 64.68 (64.90) | 4.93 (5.37) | 6.86 (6.49) | – – |
| **II** | $H_2L_b$ | $C_{21}H_{19}N_3S_2$ | 377.53 | 62.30 | Yellow | 164 | 66.81 (67.26) | 5.07 (4.73) | 11.13 (11.56) | – – |
| (**1**) | $[Co_2(L_a)(H_2O)_2]$ | $C_{22}H_{20}N_2O_4S_2Co_2$ | 558.40 | 60.66 | Yellow | >250 | 47.32 (47.79) | 3.61 (4.02) | 5.02 (4.56) | 21.11 (20.83) |
| (**2**) | $[Ni_2(L_a)(H_2O)_4]\cdot 2H_2O$ | $C_{22}H_{28}N_2O_8S_2Ni_2$ | 629.99 | 58.27 | Green | >250 | 41.94 (42.84) | 4.47 (4.68) | 4.44 (4.53) | 18.63 (18.18) |
| (**3**) | $[Cu_2(L_a)(H_2O)_2]\cdot H_2O$ | $C_{22}H_{22}N_2O_5S_2Cu_2$ | 585.64 | 67.28 | Violet | >250 | 45.12 (44.67) | 3.79 (3.46) | 4.78 (5.26) | 21.70 (22.34) |
| (**4**) | $[Zn_2(L_a)(H_2O)_2]\cdot 3H_2O$ | $C_{22}H_{26}N_2O_7S_2Zn_2$ | 625.36 | 56.62 | White | >250 | 42.25 (42.51) | 4.19 (3.74) | 4.48 (4.97) | 20.91 (21.37) |
| (**5**) | $[(VO)_2(L_a)(H_2O)_2]\cdot H_2O$ | $C_{23}H_{25}N_2O_7S_2V_2$ | 607.47 | 84.13 | Dark green | >250 | 45.48 (45.27) | 4.15 (4.63) | 4.61 (4.17) | – – |
| (**6**) | $[Ru_2(L_a)(Cl)_2(H_2O)_4]$ | $C_{22}H_{24}N_2O_6S_2Cl_2Ru_2$ | 749.61 | 63.67 | Black | >250 | 35.25 (34.75) | 3.23 (2.78) | 3.74 (3.97) | – (–) |
| (**7**) | $[Co_2(L_b)(H_2O)_5(NO_3)_2]\cdot H_2O$ | $C_{21}H_{29}N_5O_{12}S_2Co_2$ | 725.48 | 74.32 | Green | >250 | 34.76 (34.75) | 4.02 (4.75) | 9.65 (9.26) | 16.17 (17.05) |
| (**8**) | $[Ni_2(L_b)(H_2O)_3(NO_3)_2]\cdot 2H_2O$ | $C_{21}H_{27}N_5O_{11}S_2Ni_2$ | 706.99 | 81.73 | Green | >250 | 35.67 (35.18) | 3.84 (3.46) | 9.90 (10.33) | 16.60 (17.32) |
| (**9**) | $[Cu(L_b)]\cdot 3H_2O$ | $C_{21}H_{23}N_3O_3S_2Cu$ | 493.10 | 63.24 | Pale blue | >250 | 51.15 (50.67) | 4.70 (4.36) | 8.52 (8.98) | 12.89 (13.48) |
| (**10**) | $[Zn(L_b)(H_2O)]\cdot H_2O$ | $C_{21}H_{21}N_3O_2S_2Zn$ | 476.93 | 61.32 | White | >250 | 52.89 (52.47) | 4.44 (4.91) | 8.81 (8.38) | 13.71 (14.26) |
| (**11**) | $[(VO)(L_b)]\cdot 2H_2O$ | $C_{21}H_{21}N_3O_3S_2V$ | 478.49 | 64.64 | Green | >250 | 52.71 (53.08) | 4.42 (4.16) | 8.78 (9.23) | – – |
| (**12**) | $[Ru(L_b)(Cl)]\cdot 2H_2O$ | $C_{21}H_{21}ClN_3O_2RuS_2$ | 548.07 | 67.79 | Black | >250 | 46.02 (45.58) | 3.86 (4.35) | 7.67 (7.83) | – – |

Table 2. Infrared frequencies of the characteristic bands of the Schiff base ligands $H_2L_a$ and $H_2L_b$ and their transition metal complexes.

| Ligand/ complex | $\nu$(OH) | $\nu$(NH) | $\nu$(SH) | $\nu$(C=N) and $\nu$(C=C) | Py-ring | $\nu$(M–O) | $\nu$(M–N) | $\nu$(M–S) | Other assignments |
|---|---|---|---|---|---|---|---|---|---|
| **I** | 3050–3300 m | 3216 m | 2560 s | 1638 s | – | – | – | – | – |
| **II** | – | 3244 m | 2523 s | 1642 s | 995 m | – | – | – | – |
| (**1**) | 3467 s, br | – | – | 1619 s | 1019 m | 562 m | 447 m | 371 m | Neutral complex |
| (**2**) | 3346 s, br | – | – | 1600 s | 1013 m | 582 m | 456 m | 356 w | Neutral complex |
| (**3**) | 3483 s, br | – | – | 1608 s | 1028 m | 556 s | 467 m | 375 m | Neutral complex |
| (**4**) | 3362 s, br | – | – | 1616 s | 1014m | 546 m | 438 m | 369 m | Neutral complex |
| (**5**) | 3494 s, br | – | – | 1594 s | 1025 m | 568 m | 460 m | 380 m | Neutral complex, 970 m, $\nu$(VO) |
| (**6**) | 3396 s, br | – | – | 1614 s | 1023 m | 556 m | 451 m | 361 m | Neutral complex, 324 w, $\nu$ (Ru–Cl) |
| (**7**) | 3472 s, br | – | – | 1586 s | 1011 m | 563 m | 464 m | 378 w | 1374 s, 1323 s, 778 w unidentate coordinated $NO_3$ group |
| (**8**) | 3434 s, br | – | – | 1569 s | 1030 m | 550 m | 459 m | 366 m | 1452 s, 1376 s, 823 w unidentate coordinated $NO_3$ group |
| (**9**) | 3368 s, br | – | – | 1596 s | 1008 m | – | 446 m | 369 m | Neutral complex |
| (**10**) | 3490 s, br | – | – | 1606 s | 1017 m | M 543 | 440 m | 372 m | Neutral complex |
| (**11**) | 3353 s, br | – | – | 1578 s | 1021 m | 571 m | 435 m | 374 m | Neutral complex, 990 m, $\nu$(VO) |
| (**12**) | 3462 s, br | – | – | 1594 s | 1015 m | – | 456 m | 382 m | Neutral complex, 332 w, $\nu$ (Ru–C) |

Notes: s, strong; m, medium; w, weak; br, broad; $\nu_s$, a single degenerate state which is symmetrical about the principle axis; $\nu_{as}$, antisymmetrical state with respect to the three $C_{2v}$ axis; $\nu_s'$, a symmetrical state with respect to the three $C_{2v}$ axes.



($\beta$) and ligand field splitting energy (10 Dq) for complex (**7**) were calculated (*35*). The $B'$ value is lower than the free ion value ($B' = 971\,cm^{-1}$) which is an indication of orbital overlapping and delocalization of d-orbital. The nephelauxetic parameter, $\beta = B_{complex}/B_{free\ ion}$, value obtained is less than unity, suggesting a considerable cobalt–ligand bond character (Table 3).

The measured molar conductance of the $[Co_2(L_a)(H_2O)_2]$ complex (**1**) is $10\,\Omega^{-1}\,cm^2\,mol^{-1}$, indicating the non-electronic nature of the complex. On the other hand, the molar conductance value for $[Co_2(L_b)(H_2O)_5(NO_3)_2]\cdot H_2O$ complex (**7**) is $157\,\Omega^{-1}\,cm^2\,mol^{-1}$, which is higher than the expected value, since the complex is neutral. The higher value may be due to the fact that the DMF solvent replaced the $NO_3^-$ anion in the complexes, which results in the 1:2 electrolytes due to the uncoordinated nitrate ion (*36*).

The electronic spectra of the green $[Ni_2(L_a)(H_2O)_4]\cdot 2H_2O$ complex (**2**) showed two bands at 672 and 532 nm with a magnetic moment at 3.25 $\mu_B$ corresponding to the octahedral configuration. Usually, the spectra of octahedral Ni(II) consist of three transitions, assigned as $^3T_{2rmg}(F) \leftarrow {}^3A_{2g}(F)$, $^3T_{1g}(F) \leftarrow {}^3A_{2g}(F)$ and $^3T_{1g}(P) \leftarrow {}^3A_{2g}(F)$. The last transition $^3T_{1g}(P) \leftarrow {}^3A_{2g}(F)$ was not observed as its position should be near IR and is out of the instrument used. The ligand field parameters (10 Dq, $B$ and $\beta$) were calculated and found in the range reported for the proposed structure. For $[Ni_2(L_b)(H_2O)_3(NO_3)_2]\cdot 2H_2O$ (**8**), the absorption bands were observed at 730 and 396 nm, which are attributed to the $^3T_{1g}(F) \leftarrow {}^3A_{2g}(F)$ and $^3T_{1g}(F) \leftarrow {}^3A_{2g}(F)$ transitions, respectively, in an octahedral geometry (*37*). An additional broad band is also observed around 478 nm in the spectrum of the complex which may be due to the existence of the square planar configuration around the other Ni(II) ion. The ligand field parameters were calculated. The values are lower than that reported for a regular octahedral, proving the suggested distorted

Table 3. Electronic absorption bands (nm), their transition assignment, ligand field parameters, magnetic moments (B.M.) and molar conductivities of the Schiff base ligands ($H_4L_a$ and $H_2L_b$) and their transition metal complexes.

| Complex | | d–d Transition, (nm) and their assignments | | Ligand field parameters | | | Magnetic moment($\mu_B$) | | |
|---|---|---|---|---|---|---|---|---|---|
| | | | | $B$(cm$^{-1}$) | $\beta$ | 10 Dq(cm$^{-1}$) | $\mu^{a}_{complex}$ | $\mu^{b}_{eff}$ | ($\Lambda^{c}$) |
| (**1**) | $[Co_2(L_a)(H_2O)_2]$ | 534 (0.43) | $^2A_{1g} \leftarrow {}^2B_{2g}$ | – | – | – | 2.17 | 1.87 | – |
| (**2**) | $[Ni_2(L_a)(H_2O)_4]\cdot 2H_2O$ | 613 (0.67) | $^3T_{2g}(F) \leftarrow {}^3A_{2g}(F)$ | 683 | 0.654 | 10.243 | 4.68 | 3.25 | 13 |
| | | 514 (0.38) | $^3T_{1g}(F) \leftarrow {}^3A_{2g}(F)$ | | | | | | |
| (**3**) | $[Cu_2(L_a)(H_2O)_2]\cdot H_2O$ | 578(0.56) | $^2B_{1g} \rightarrow {}^2E_g$ | – | – | – | 1.73 | 1.38 | 16 |
| | | 695(0.27) | $^2B_{1g} \rightarrow {}^2A_{1g}$ | | | | | | |
| (**4**) | $[Zn_2(L_a)(H_2O)_2]\cdot 3H_2O$ | – | – | – | – | – | – | – | 21 |
| (**5**) | $[(VO)_2(L_a)(H_2O)_2]\cdot H_2O$ | 775 (0.82) | $^2B_{2g} \leftarrow {}^2E_2(\upsilon_2)$ | – | – | – | 1.83 | 1.83 | 13 |
| (**6**) | $[Ru_2(L_a)(Cl)_2(H_2O)_4]$ | 690 (0.54) | $^2T_{2g} \rightarrow {}^2A_{2g}$ | – | – | – | – | – | – |
| | | 553 (0.65) | $^2T_{2g} \rightarrow {}^2E_g$ | | | | | | |
| (**7**) | $[Co_2(L_b)(H_2O)_5(NO_3)_2]\cdot H_2O$ | 558 (0.21) | $^4A_{2g}(F) \leftarrow {}^4T_{1g}(F)$ | 863 | 0.780 | 4365 | 5.16 | 4.34 | 157 |
| | | 665 (0.54) | $^4T_{1g}(P) \leftarrow {}^4T_{1g}(F)$ | | | | | | |
| (**8**) | $[Ni_2(L_b)(H_2O)_3(NO_3)_2]\cdot 2H_2O$ | 730 (0.52) | $^3T_{2g}(F) \leftarrow {}^3A_{2g}(F)$ | 658 | 0.647 | 10.547 | 3.68 | 2.26 | 148 |
| | | 396 (0.34) | $^3T_1(F) \leftarrow {}^3A_{2g}(F)$ | | | | | | |
| (**9**) | $[Cu(L_b)]\cdot 3H_2O$ | 625 (0.73) | $^2A_{1g} \leftarrow {}^2B_{1g}$ | – | – | – | 1.72 | 1.72 | 11 |
| (**10**) | $[Zn(L_b)(H_2O)]\cdot H_2O$ | – | – | – | – | – | – | – | 23 |
| (**11**) | $[(VO)(L_b)]\cdot 2H_2O$ | 835 (0.52) | $^2B_2 \leftarrow {}^2E(\upsilon_1)$ | – | – | – | 1.54 | 1.54 | 12 |
| | | 626 (0.76) | $^2B_2 \leftarrow {}^2B_2(\upsilon_2)$ | | | | | | |
| (**12**) | $[Ru(L_b)(Cl)]\cdot 2H_2O$ | 654 (0.67) | $^2T_{2g} \rightarrow {}^2A_{2g}$ | – | – | – | – | – | 24 |
| | | 510 (0.56) | $^2T_{2g} \rightarrow {}^2E_g$ | | | | | | |

Notes: [a] $\mu_{complex}$ is the magnetic moment of all metals ions present in the complex. [b] $\mu_{eff}$ is the magnetic moment of one cation in the complex. Molar conductivities were measured in DMF solvent with concentration $\times 10^{-3}$ M. Values are in $\Omega^{-1}$ cm$^2$ mol$^{-1}$. [c] Values of $\varepsilon_{max}$ are in parentheses and multiplied by $10^{-4}$ (mol$^{-1}$ cm$^{-1}$).

structure. The magnetic moment value of the isolated complex (**8**) was measured and was found to be 2.26 $\mu_B$, which is a subnormal value compared with that which lies in the range reported for different stereochemistries of Ni(II) and supporting the presence of mixed stereochemistry around the Ni(II) atoms (*38*). The molar conductance values of Ni(II) complexes (**2**) and (**8**) in DMF solution were 13 and 148 $\Omega^{-1}$ cm$^2$ mol$^{-1}$, respectively, indicating the neutral nature of the complexes. The high measured value in complex (**8**) was observed as a result of the replacement of DMF by the coordinated nitrate group and the complex solution becomes 1:2 electrolyte.

$[Cu_2(L_a)(H_2O)_2]\cdot H_2O$ (**3**) is suggested to be square planar and shows two absorption bands at 578 and 695 nm which are assigned to $^2B_{1g} \rightarrow {}^2E_g$ and $^2B_{1g} \rightarrow {}^2A_{1g}$ transitions. On the other hand, the electronic spectrum of the complex (**9**) $[Cu(L_b)]\cdot 3H_2O$ exhibits a d–d transition band at 625 nm and another strong band due to S $\rightarrow$ Cu(II) metal ion as charge transfer transition at 436 nm. The measured value of the magnetic susceptibility for Cu(II) complexes was 1.48 $\mu_B$ for the former complex (**3**) and 1.72 $\mu_B$ for the latter (**9**). These values lie in the range reported for the square planar and square pyramidal geometry for complexes (**3**) and (**9**), respectively (*34*, *39*). The measured molar conductances of Cu(II) complexes in DMF solution were 16 and 11 $\Omega^{-1}$ cm$^2$ mol$^{-1}$, indicating the non-electronic nature of complexes (**3**) and (**9**).

$[Zn_2(L_a)(H_2O)_2]\cdot 3H_2O$ (**4**) and $[Zn(L_b)(H_2O)]\cdot H_2O$ (**10**) complexes are of diamagnetic nature and so there is no electronic d–d transition or significant magnetic moment. With the aid of the elemental analysis and IR spectra, the proposed configuration is expected to be tetrahedral and octahedral for complexes (**4**) and (**10**), respectively. Molar conductance values in DMF were 21 and 23 $\Omega^{-1}$ cm$^2$ mol$^{-1}$, indicating the neutral nature of these complexes.

The electronic spectra of the green vanadyl complex $[(VO)_2(L_a)(H_2O)_2]\cdot H_2O$ (**6**) exhibits one band at 775 nm, which is due to $^2B_{2g} \rightarrow {}^2E(\nu_2)$ transition characteristic of the square pyramidal geometry. The measured effective magnetic moment of the complex is 1.83 $\mu_B$, supporting the geometry of the observed electronic spectra and excluding the metal–metal interaction even in the presence of two nuclei atoms in the complex. Moreover, the band at 970 cm$^{-1}$, in the IR spectra of the vanadyl complexes, agrees well with the proposed structure (*40*). On the other hand, the spectra of complex $[(VO)(L_b)]\cdot 2H_2O$ (**12**) shows three bands at 835, 626 and 374 nm which are assigned to $^2B_2 \rightarrow {}^2E(\nu_1)$, $^2B_2 \rightarrow {}^2B_1(\nu_2)$ and $^2B_2 \rightarrow {}^2A_1(\nu_3)$ electronic transitions, respectively, characteristic of the distorted octahedral geometry around the VO(IV) ion. The value of the magnetic moment is 1.86 $\mu_B$, which is in good agreement with a $d^1$ system and is consistent with a mono-nuclear distorted octahedral geometry (*37*).

The ground state of Ru(III) is $^2T_{2g}$, and the first excited doublet levels in the order of increasing energy are $^2A_{2g}$ and $^2A_{1g}$ which arise from the $t_{2g}^4 e_g^1$ configuration. In a $d^5$ system, and especially in Ru(III) which is a relatively strong oxidizing agent, charge transfer bands of the type $L_{\pi y} \rightarrow t_{2g}$ are prominent in the low-energy region and obscure the weaker bands due to the d–d transition. The electronic spectra of Ru(III) complexes (**3**) and (**6**) exhibit mainly three bands at 690, 553 and 337 nm and 654, 510 and 395 nm, respectively. The first band is assigned to the d–d transition ($^2T_{2g} \rightarrow {}^2A_{2g}$), while the second intense band is due to M–$L_\pi$* transition ($^2T_{2g} \rightarrow {}^2E_g$). The last one is attributed to the inter-ligand transition or to MLCT bands ($^2T_{2g} \rightarrow {}^2A_{1rmg}$). The positions of the absorption bands as well as magnetic susceptibility measurements (1.72 $\mu_B$ for $[Ru_2(L_a)(Cl)_2(H_2O)_4]$ and 1.93 $\mu_B$ for $[Ru(L_b)(Cl)]\cdot 2H_2O$) indicate the presence of one unpaired electron, confirming a low-spin octahedral configuration (*37*).

### 2.3. *ESR spectra*

The X-band ESR spectra of some selected complexes have been studied in order to provide information about the hyperfine and superhyperfine structures to elucidate the geometry and the degree of covalency of the metal–ligand bonds (Figure 1). The ESR spectrum of the complex

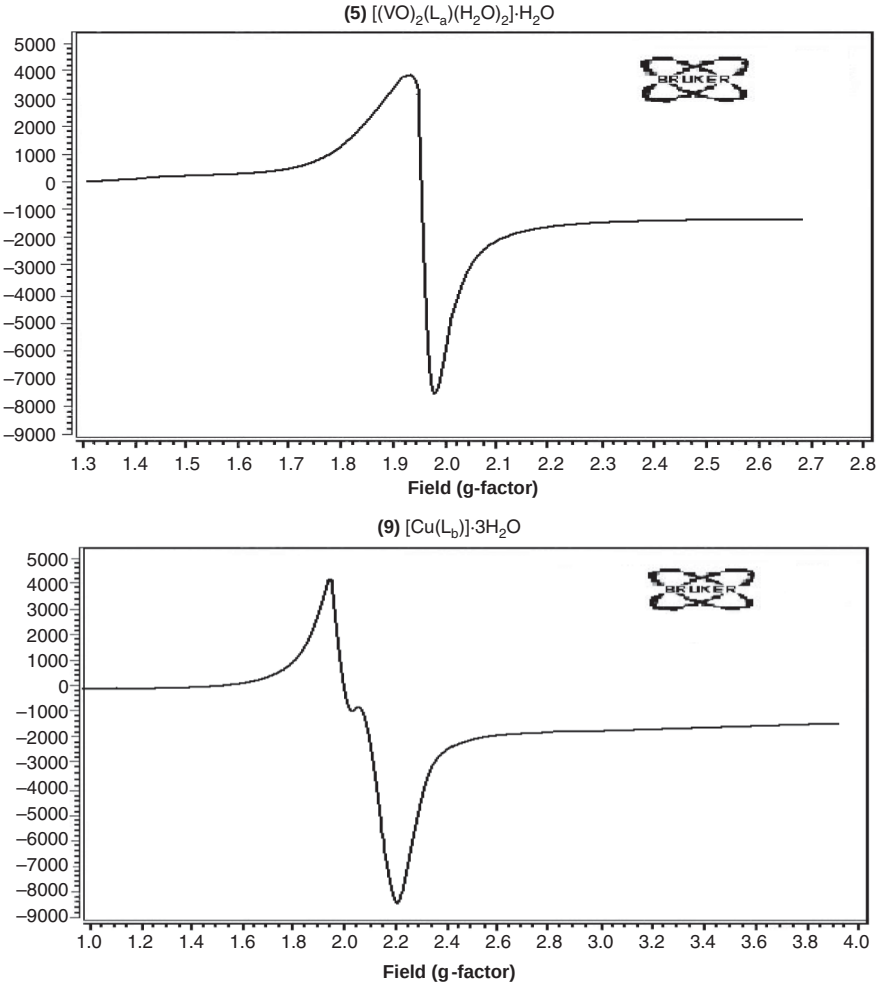


Figure 1. ESR spectra of the complexes, (**5**) $[(VO)_2(L_a)(H_2O)_2]\cdot H_2O$ and (**9**) $[Cu(L_b)]\cdot 3H_2O$.

$[Cu(L_b)]\cdot 3H_2O$ (**9**) at room temperature was recorded at a frequency of 9.7 GHz with a field set of 3250 G. The spin Hamiltonian parameters for the Cu(II) complex can be used to derive the ground state. In square planar or square pyramidal complexes, the unpaired electron lies in the $d_{x^2-y^2}$ orbital giving $^2B_{1g}$ as the ground state with $g_\parallel > g_\perp > 2.0023$, while giving $^2A_{1g}$ with $g_\perp > g_\parallel > 2.0023$, if the unpaired electron lies in the $d_{z^2}$ orbital (*41*). The observed measurements $g_\parallel(2.35) > g_\perp(2.03) > 2.0023$ indicate that the complex is axially symmetric and occupies its unpaired electron in $d_{x^2-y^2}$ orbital characteristic of the square-planar or square pyramidal geometry (*42*). Kilveson (*43*) has reported the $g_\parallel$ value as an important function for indicating the covalent character of M–L bond. For ionic and covalent characters, $g_\parallel > 2.3$ and $g_\parallel < 2.3$, respectively. In the present complex, the $g_\parallel$ is more than 2.3, indicating an appreciable covalent character for the Cu–L bond. In addition, the exchange coupling interaction between two copper centers is explained by the Hathaway (*44*) expression: if the value of $G$ is greater than 4, the exchange interaction in the solid state is negligible, whereas when it is less than 4, a considerable exchange interaction is noticed in the solid complex. The calculated $G$-value of the complex suggests some interaction between Cu(II) centers (*45*). The elemental analysis, the electronic spectra as well

as the positions of the bands and the shape of ESR spectra agree well with the formation of the square pyramidal geometry for the Cu(II) complex.

The ESR spectra of $[(VO)_2(L_a)(H_2O)_2]\cdot H_2O$ (**5**) complex exhibit a single asymmetric line centered at $g = 1.97$ without a resolved hyperfine structure. The absence of vanadium hyperfine coupling is common in solid state samples (*46*). This behavior is attributed to the simultaneous flipping of neighboring electron spins or due to strong exchange interactions. Upon the pairing of two vanadyl ions, the two electrons' spins may combine to a non-magnetic spin singlet ($S = 0$) or to a paramagnetic spin triplet state ($S = 1$), only the latter is observed in the spectra. The super exchange interaction between the two vanadium ions leads to a configuration in which the two electron spins have a strong interaction. A square pyramidal geometry is proposed for the binuclear complex (*47*).

### 2.4. $^1$*H-NMR spectra of Zn (II) complexes*

The $^1$H-NMR spectra of thio-Schiff base ligands $H_4L_a$ and $H_2L_b$ in dimethyl-sulfoxide (DMSO-$d_6$), without and with $D_2O$. Their chemical shifts (ppm) and assignments are listed in Table 4. The signals at 2.48 and 2.32 ppm are assigned to the protons of the methyl groups for $H_4L_a$ and $H_2L_b$, respectively. On the other hand, a triplet single at 7.23 and a doublet at 8.10 ppm correspond to the protons of pyridine moiety for the $H_2L_b$ ligand. The proton resonance of the hydroxyl groups (10.21 ppm) as well as thiol groups (3.32 ppm) for $H_4L_a$ ligands and the signals of the thiol groups for $H_2L_b$ (3.37 ppm) disappeared in the presence of $D_2O$, which indicate that these protons are acidic. The absence of resonances for OH/SH protons in the spectra of $[Zn_2(L_a)(H_2O)_2]\cdot 3H_2O$ (**4**) and $[Zn(L_b)(H_2O)]\cdot H_2O$ (**10**) complexes indicates the deprotonation of the phenolic/thiophenolic group of the Schiff bases and coordination of the oxygen and sulfur atoms through the coordination to the metal atom. It is noticeable that the signals due to the pyridine moiety protons show a remarkable shift in $[Zn(L_b)(H_2O)]\cdot 3H_2O$ complex suggesting the involvement of the pyridine nitrogen with the metal ion. Moreover, in the spectra of diamagnetic Zn(II) complexes (**4**) and (**10**), the protons of the methyl group bonded to the azomethine groups are shifted downfield compared with that of the free ligand as a result of chelation of the azomethine group through coordination via metal ion (Figure 2). The broad bands of the aromatic protons of the Schiff bases moiety appeared at the same position on complexation (*48*).

### 2.5. *Thermal gravimetric analysis*

TGA studies were carried out to illustrate the thermal stability of the complexes and to investigate whether the water molecules are in the inner or outer coordination sphere of the central metal ion (Figure 3) (*49*). TGA curve of $[Cu_2(L_a)(H_2O)_2]\cdot H_2O$ (**3**) shows that the first stage of decomposition is at 56–127°C with the elimination of one crystalline water molecule of the total weight of the complex (Calc./Found %: 3.07/3.34%). The second stage at the range 130–233°C corresponds to the removal of two coordinated water molecules (Calc./Found %: 6.15/5.87%). The last stage within the temperature range from 233 to 736°C can be assigned to the loss of 64.00% of the total weight of the complex as a result of the removal of the fragment part of the ligand and the formation of copper oxide (Calc./Found %: 27.17/26.79%). DrTGA curve of the complex shows two endothermic peaks. The first at 116°C is due to the removal of crystalline water molecule, while the peak at 215°C is due to the loss of coordinated water molecules. The last endothermic peak at 687°C is ascribed to the decomposition of the anhydrous complex (Scheme 3), depicting the thermal degradation pattern of the complex as follows:

On the other hand, the TGA–DrDTA curve for complex (**8**), $[Ni_2(L_b)(H_2O)_3(NO_3)_2]\cdot 2H_2O$, displays four degradation steps of decomposition. The former stage in the range of 64–136°C is

Table 4. $^1$H-NMR chemical shifts ($\delta$, ppm) of the Schiff base, $H_4L_a$ and $H_2L_b$, ligands and their Zn(II) complexes (**4**) and (**10**) in DMSO-$d_6$ after the addition of $D_2O$.

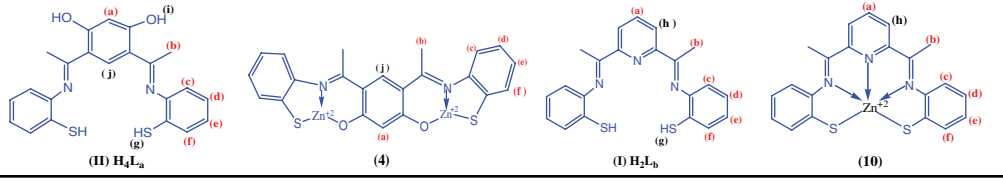


| Assignment | | Chemical shifts, $\delta_H$ | | | | Complexes | |
|---|---|---|---|---|---|---|---|
| | | $H_4L_a$ | $H_4L_a$ ($D_2O$) | $H_2L_b$ | $H_2L_b$ ($D_2O$) | (**4**) $[Zn_2(L_a)(H_2O)_2]\cdot 3H_2O$ | (**10**) $[Zn(L_b)(H_2O)]\cdot H_2O$ |
| (**1**) | $H^a$ [t, 1H, Ar–H] | 6.24 | 6.24 | 7.23 | 7.23 | 6.31 | 7.25 |
| (**2**) | $H^b$ [s, 6H, $2CH_3$] | 2.48 | 2.48 | 2.32 | 2.32 | 2.53 | 2.39 |
| (**3**) | $H^c$ [d, 2H–Ar] | 7.68 | 7.68 | 7.59 | 7.59 | 7.63 | 7.59 |
| (**4**) | $H^d$ [t, 2H–Ar] | 6.58 | 6.58 | 6.62 | 6.62 | 6.58 | 6.62 |
| (**5**) | $H^e$ [t, 2H–Ar] | 7.25 | 7.25 | 7.21 | 7.21 | 7.25 | 7.20 |
| (**6**) | $H^f$ [d, 2H–Ar] | 6.42 | 6.42 | 6.79 | 6.79 | 6.42 | 6.78 |
| (**7**) | $H^g$ [s, 2H] | 3.32 | – | 3.37 | – | – | – |
| (**8**) | $H^h$ [d, 2H–Ar] | – | – | 8.10 | 8.10 | – | 8.22 |
| (**9**) | $H^i$ [s, br, 2H, 2–OH] | 10.21 | – | – | – | – | – |
| (**10**) | $H^j$ [s, 1H, Ar–H] | 8.36 | 8.36 | – | – | 7.98 | – |

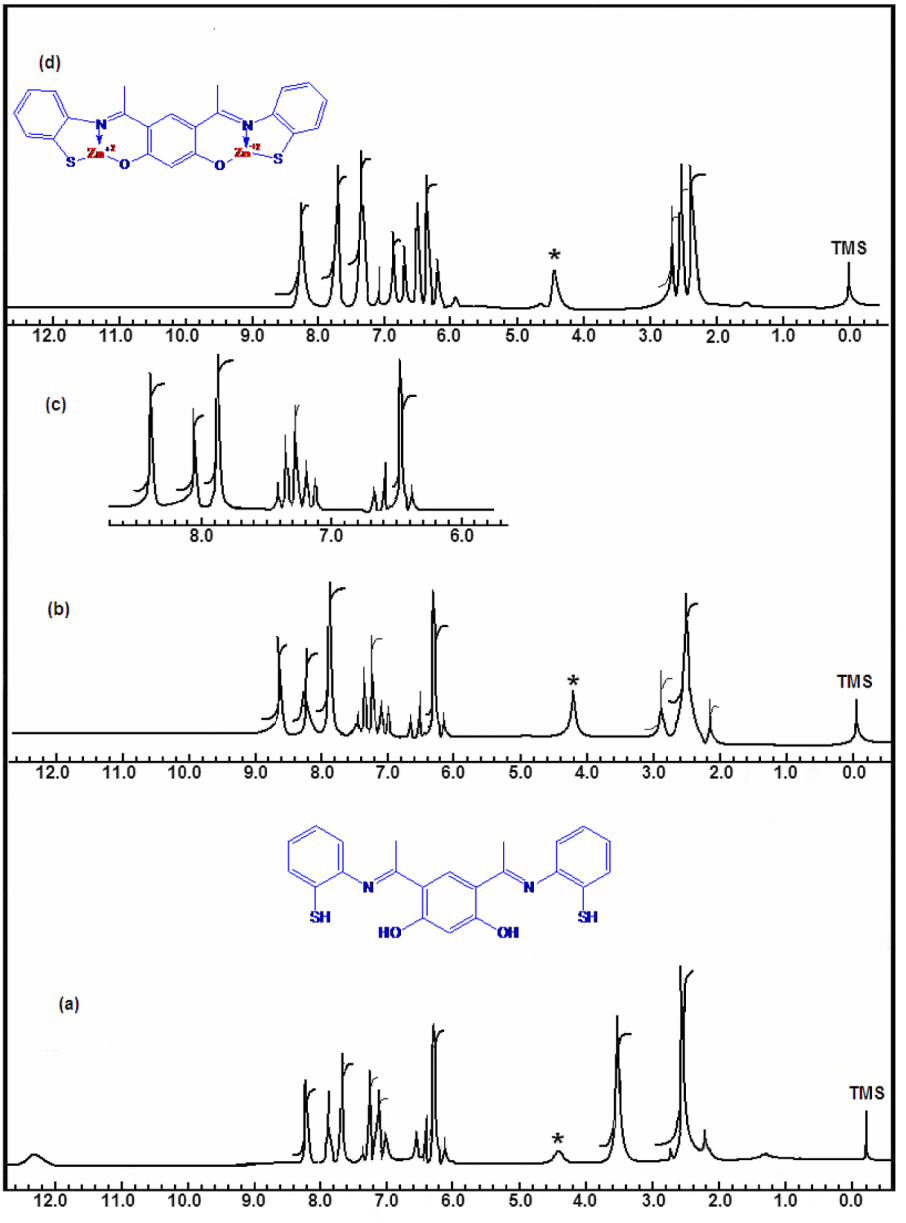


Figure 2. $^1$H-NMR spectra ($\delta$, ppm) in DMSO-$d_6$ solvent of the (a) Schiff base, ligand $H_4L_a$ (b) Schiff base, $H_4L_a$, ligand after the addition of $D_2O$. (c) Expansion to the range, 5.5–8.5 ppm from the spectrum of $H_4L_a$ (d) $^1$H-NMR spectra ($\delta$, ppm) in DMSO-$d_6$ solvent of the complex, $[Zn_2(L_a)(H_2O)_2] \cdot 3H_2O$ (*suppressed solvent).

due to the loss of the crystalline water molecules, (weight loss; Calc./Found %: 5.09/6.45%). The second stage at the range 140–232°C ascribed to the loss of three coordinated water molecules of the total weight of the complex (weight loss; Calc./Found %: 7.64/6.37%). The third stage observed in the range 243–387°C corresponds to the evolution of $N_2O_5$ molecules, with weight loss (Calc./Found %: 15.27/14.31%). The removal of the fragment part of the ligand occurred in the temperature range at 387–738°C, accompanied by weight loss (Calc./Found %: 53.05/52.24%), as a result of the complete decomposition and the formation of the nickel oxide as a residue

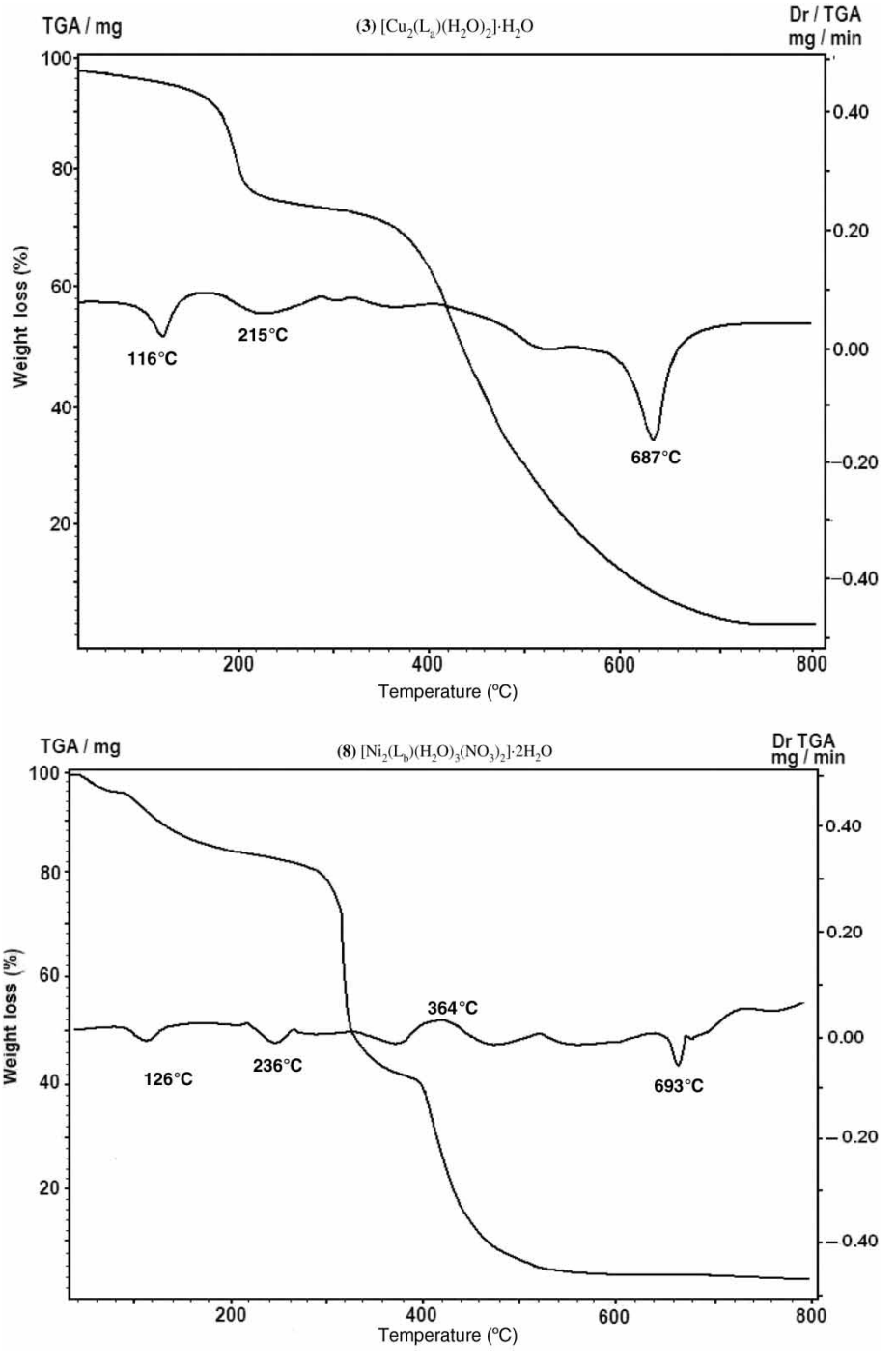


Figure 3. TGA/DrTGA curve of complex (**3**) $[Cu_2(L_a)(H_2O)_2]\cdot H_2O$ and (**8**) $[Ni_2(L_b)(H_2O)_3(NO_3)_2]\cdot 2H_2O$.

$$[Cu_2(L_a)(H_2O)_2]\cdot H_2O \xrightarrow[56\text{–}127^\circ C]{-H_2O} [Cu_2(L_a)(H_2O)_2] \xrightarrow[130\text{–}233^\circ C]{-2H_2O} [Cu_2(L_a)] \xrightarrow[233\text{–}736^\circ C]{(-L_a)} \text{Copper oxide}$$

Scheme 3. Thermal degradation pattern of $[Cu_2(L_a)(H_2O)_2]\cdot H_2O$, complex (**3**).

(20.63%). DrTGA curve of the complex shows endothermic peaks at 126°C and 187°C as a result of the loss of crystalline and coordinated water molecules, respectively. On the other hand, an exothermic peak observed at 364°C which is due to the loss of $N_2O_5$ molecules and the last endothermic peak at 639°C which is ascribed to the complete decomposition of the complex (Scheme 4) depict the thermal degradation pattern of the complex in the range 50–800°C.

$$[Ni_2(L_b)(H_2O)_3(NO_3)_2]\cdot 2H_2O \xrightarrow[64\text{–}136^\circ C]{-2H_2O} [Ni_2(L_b)(H_2O)_3(NO_3)_2] \xrightarrow[140\text{–}232^\circ C]{-3H_2O} [Ni_2(L_b)(NO_3)_2] \xrightarrow[343\text{–}387^\circ C]{-N_2O_5} [Ni_2(L_b)] \xrightarrow[387\text{–}738^\circ C]{-L_b} \text{Nickel oxide}$$

Scheme 4. Thermal degradation pattern of $[Ni_2(L_b)(H_2O)_3(NO_3)_2]\cdot 2H_2O$, complex (**8**).



### 2.6. *Antimicrobial activities*

Schiff bases and their corresponding transition metals were found to possess appreciable fungicidal and bactericidal properties against bacteria such as *Rhizobium* and *Azotobacter* and fungi such as *Aspergillus niger* and *Fusarium oxysporium*). The results are summarized in Table 5. The ligands and the complexes showed varying degrees of inhibitory effect on the growth of the bacterial/or fungal strains tested (*50*, *51*). It was observed from the results that the activity of complexes is much higher than that of the corresponding ligands (Figure 4). This enhancement of the activity can be rationalized on the basis of their structures possessing an additional C=N bond. Furthermore,

Table 5. Antibacterial activity and antifungal activity data of the ligand and its transition metal complexes.

| | | % Zone diameter showing complete growth inhibition | | | |
|---|---|---|---|---|---|
| | | Antibacterial activity | | Antifungal activity | |
| Item | Ligand/complex | *Rhizobium* | *Azotobacter* | *A. niger* | *F. oxysporium* |
| **I** | $H_4L_a$ | 53 | 48 | 38 | 43 |
| **II** | $H_2L_b$ | 58 | 52 | 45 | 47 |
| (**1**) | $[Co_2(L_a)(H_2O)_2]$ | 62 | 56 | 46 | 48 |
| (**2**) | $[Ni_2(L_a)(H_2O)_4]\cdot 2H_2O$ | 58 | 62 | 58 | 46 |
| (**3**) | $[Cu_2(L_a)(H_2O)_2]\cdot H_2O$ | 67 | 57 | 48 | 45 |
| (**4**) | $[Zn_2(L_a)(H_2O)_2]\cdot 3H_2O$ | 58 | 56 | 41 | 47 |
| (**5**) | $[(VO)_2(L_a)(H_2O)_2]\cdot H_2O$ | 66 | 58 | 50 | 48 |
| (**6**) | $[Ru_2(L_a)(Cl)_2(H_2O)_4]$ | 67 | 57 | 55 | 47 |
| (**7**) | $[Co_2(L_b)(H_2O)_5(NO_3)_2]\cdot H_2O$ | 63 | 54 | 55 | 46 |
| (**8**) | $[Ni_2(L_b)(H_2O)_3(NO_3)_2]\cdot 2H_2O$ | 71 | 56 | 56 | 50 |
| (**9**) | $[Cu(L_b)]\cdot 3H_2O$ | 61 | 58 | 52 | 43 |
| (**10**) | $[Zn(L_b)(H_2O)]\cdot H_2O$ | 71 | 58 | 56 | 46 |
| (**11**) | $[(VO)(L_b)]\cdot 2H_2O$ | 69 | 61 | 54 | 43 |
| (**12**) | $[Ru(L_b)(Cl)]\cdot 2H_2O$ | 73 | 63 | 58 | 58 |

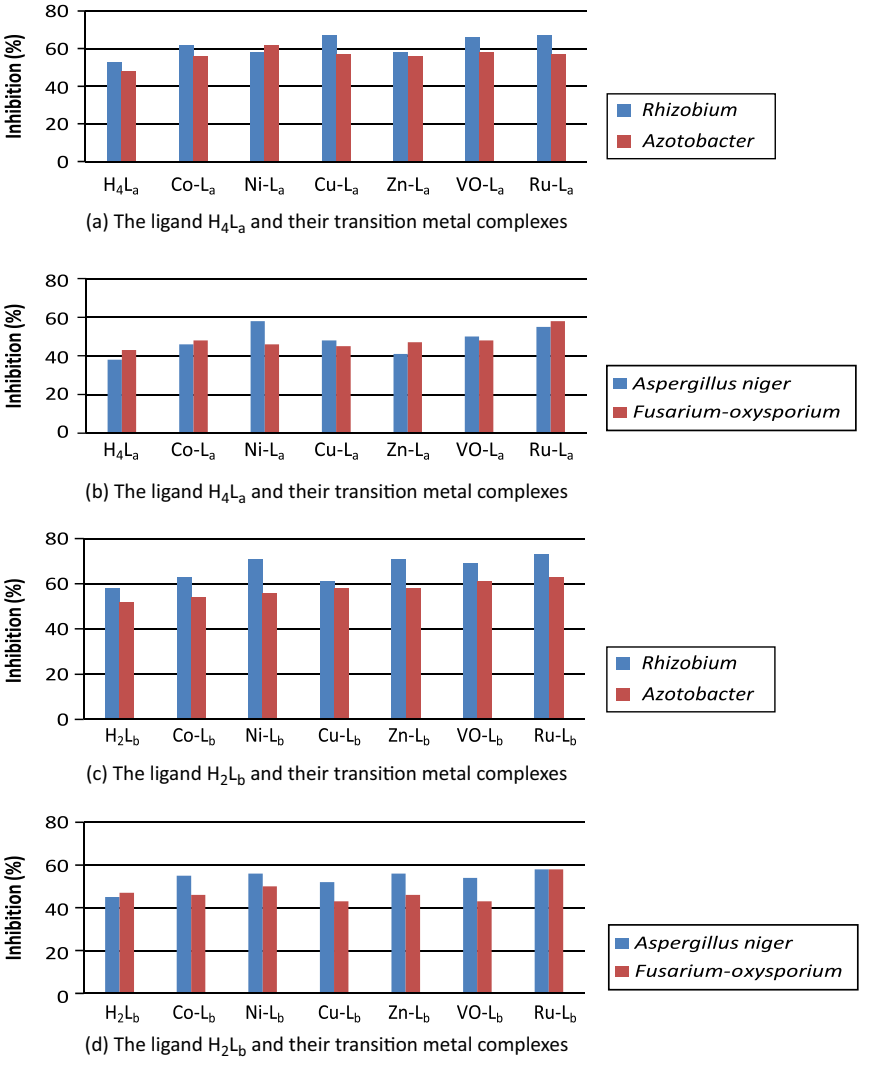


Figure 4. Biological activity data of Schiff base ligands, $H_4L_a$ and $H_2L_b$ and their transition metal complexes against antibacterial and antifungal activity.

coordination reduces the polarity of the metal ion mainly because of the partial sharing of its positive charge with these donor groups and possibly because of the $\pi$-electron delocalization within the whole chelate ring system. Thus, the chelation increases the lipophilic nature of the central metal atom, which in turn favors its permeation through the lipid layer of the membrane of the microorganisms' cell wall more effectively, thus raising the activity of the drug.

## 3. Conclusion

The reaction of ABT with DAR or DAP in the molar ratio 2:1 forms two Schiff bases $H_4L_a$ and $H_2L_b$ which reacted with the transition metal ions Co(II), Ni(II), Cu(II), Zn(II), VO(IV) and Ru(III) to afford the corresponding complexes which exhibit mono- or binuclear structures of distorted octahedral, tetrahedral, square planar or square pyramid structure where the $H_4L_a$ ligand behaves

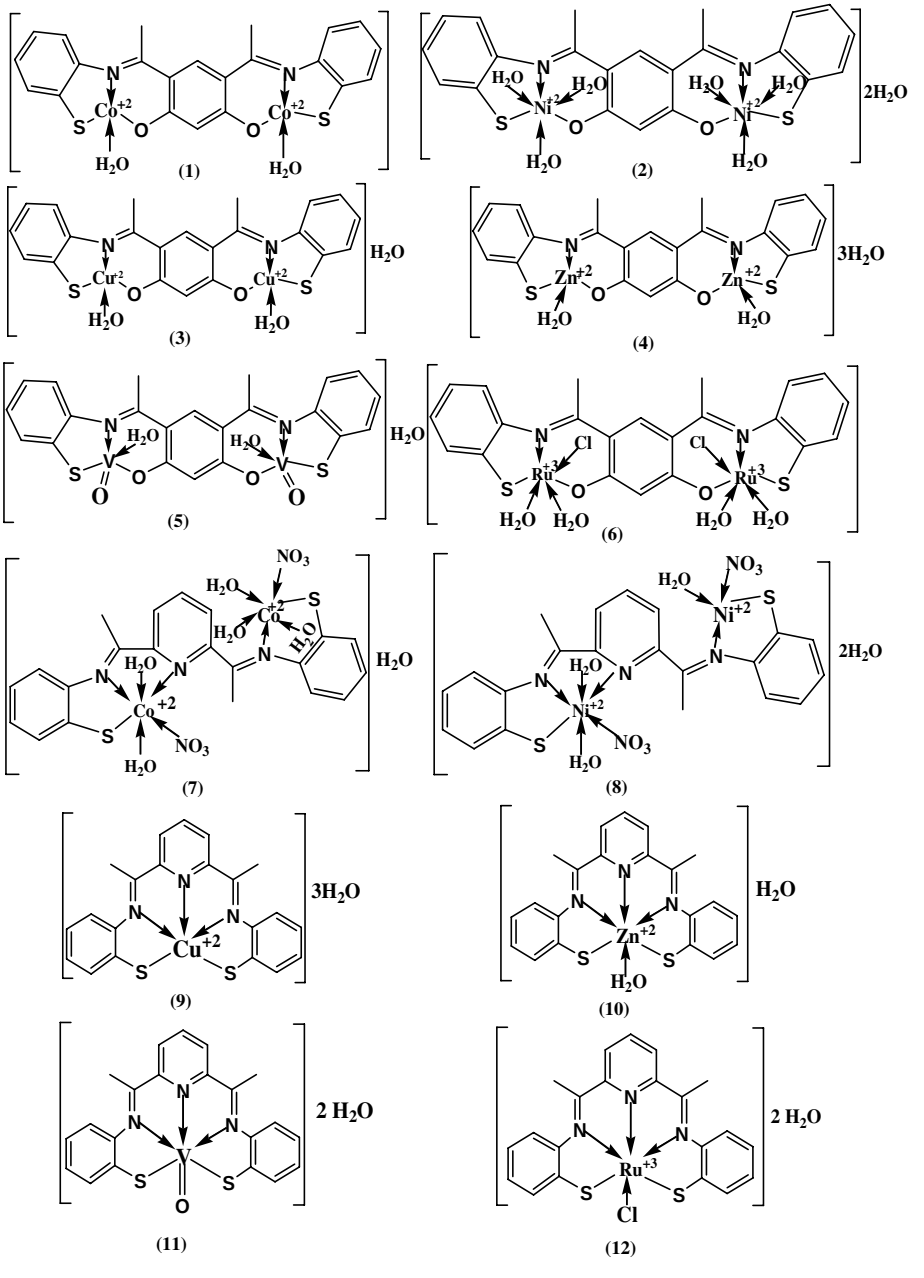


Figure 5. Representative structures of the metal complexes of the Schiff bases $H_4L_a$ and $H_2L_b$.

as a tetrabasic hexadendate ligand while $H_2L_b$ behaves as a dibasic pentadentate ligand. The bonding sites are azomethane, sulfur atoms and phenolic oxygen for $H_4L_a$ or pyridine nitrogen for $H_2L_b$. Figure 5 depicts the representative structures of the metal complexes on the basis of the elemental analysis, electronic spectral measurements and magnetic susceptibility data. TGA suggests high stability for the complexes, showed thermal decomposition in different stages and confirmed the presence of crystalline or coordinated water molecules.

## 4. Experimental

### 4.1. *Materials*

The nitrate salts of Co(II), Ni(II), Cu(II) and Zn(II) were Merck or BDH·$RuCl_3$·$3H_2O$ was purchased from Labo Chemie France. VO(IV) acetate and DAP were from Aldrich. Resorcinol, acetic anhydride, zinc chloride and 2-aminobenzothiazole were supplied from Merck Chemicals. Organic solvents were reagent grade chemicals.

### 4.2. *Physical measurement*

Microanalyses of carbon, hydrogen and nitrogen were carried out at the micro-analytical Center, Cairo University, Egypt. Analyses of the metals in the solid complex have been carried out by using EDTA (*52*). Electronic spectra of the metal complexes as solid reflecting were measured on a Perkin-Elmer 2400 series II analyzer, and spectra of the compounds in KBr pellets in the range 4000–400 range were obtained with a Perkin-Elmer, FTIR model 8101 spectrophotometer. The UV–VIS spectra of the complexes were obtained on a Jasco model v-550 spectrophotometer. $^1$H-NMR spectra were recorded using a Varian genini-300 MHz spectrophotometer 90 MHz. DMSO-$d_6$ was added as a solvent and tetramethylsilane as an internal reference. $D_2O$ was added to every sample to test for the deuteration of the complexes. Abbreviations are: s = singlet, d = doublet, t = triplet and m = multiple. Magnetic susceptibilities of the complexes were measured at room temperature using a Johnson Matthey, Alfa Products, model MKI magnetic susceptibility balance. The effective magnetic moments were calculated from the expression $\mu_{\text{eff.}} = 2.828(\chi_{\text{M}} \cdot \text{T})^{1/2}$ B.M., where $\chi_{\text{M}}$ is the molar susceptibility corrected using Pascal's constants for the diamagnetism of all atoms in the compounds (*53*). A TGA/DTA thermal analyzer was manufactured by using NETZSCH-gerateban Bestell – Nr 348472c. The thermal analyzer was equipped with a thermobalance. Samples (∼50 mg) were heated at a programmed rate of 20°C $min^{-1}$ in a dynamic $N_2$ atmosphere. The sample was contained in a boat-shaped platinum pan suspended in the center of a furnace. ESR spectra of the copper complexes were recorded on a JEOL microwave unit, JES-$FE_2$XG Spectrometer, at the National Research Centre, Giza, Egypt. Molar conductances of $10^{-3}$ M solutions of the complexes in DMF were measured with the Corning conductivity meter NY 14831 model 441 (USA).

### 4.3. *Synthesis of the Schiff base*

#### 4.3.1. *Schiff base, 4,6-bis((E)-1-(2-mercaptophenylimino)ethyl) benzene-1,3-diol, $H_4L_a$*

The Schiff base $H_4L_a$ was prepared in two steps. The first step is the preparation of DAR by acetylating resorcinol (5.00 g, 45.5 mmol) with acetic anhydride (9.28 g, 91.0 mmol) in the presence of excess zinc chloride (10.0 g, 73.4 mmol) at 140°C in a paraffin oil path. The hot mixture was cooled to room temperature and poured onto 140 ml of 50% dilute hydrochloric acid. Orange precipitate was formed and increased with standing until 1 h. The orange crude product was obtained by filtration with suction and washed with distilled water till the color of the filtrate is nearly colorless. Orange needle crystals were obtained by crystallization using either ethanol or acetic acid/water mixture (*54*). The second step is the addition of a solution of ABT (2.25 g, 9.015 mmol) in ethanol (30 ml) to ethanolic solution of DAR (1.75 g, 9.00 mmol, 40 ml ethyl alcohol), corresponding to the molar ratio 2:1, respectively. The solutions were refluxed for 3 h. A yellow ($H_4L_a$) ligand was formed on cooling the solutions slowly to room temperature and the precipitates were collected by filtration, washed with ethanol then diethyl ether and finally air-dried. The yield was 2.68 g (68.71%) and the m.p. is 182°C for $H_4L_a$.

#### 4.3.2. *Schiff base, 2-((E)-1-(6-((E)-1-(2-mercaptophenylimino) ethyl) pyridine-2-yl) ethylideneamino) benzenthiol, $H_2L_b$*

A solution of ABT (2.68 g, 10.725 mmol) in ethanol (30 ml) was added to DAP (1.75 g, 10.725 mmol) in ethanol (40 ml) in the molar ratio 2:1 and the solutions was refluxed for 3 h. Yellow ($H_2L_b$) crystals were formed on cooling the solutions slowly to room temperature and the precipitate was collected by filtration, washed with ethanol then diethyl ether and finally air-dried. The yield was 2.76 g (62.30%) and the m.p. is 164˚C for $H_2L_b$.

### 4.4. *Synthesis of the transition metal complexes of the Schiff base ligands $H_4L_a$ and $H_2L_b$*

Ethanolic solutions of $H_4L_a$ and $H_2L_b$ ligands were added gradually to ethanolic solutions of the metal nitrates in the molar ratio 1:2. The reaction mixtures were stirred for 30 min and then they were refluxed for 2 h. Most of the complexes were formed during the reflux. The products were isolated by filtration and washed with several portions of ethanol, then ether and air-dried. The complexes are insoluble in most common organic solvents, but soluble in DMF and/or DMSO. In the preparation of VO(IV) complexes, 0.1 g of sodium acetate was added as a buffering agent to raise the pH medium. The following detailed preparations are given as examples and the other complexes were obtained similarly. Reaction of the $H_2L_b$ ligand with few metals in the molar ratio 1:2 was not successful in most cases to afford the corresponding binuclear mole ratio where Cu(II), Zn(II), Ru(III) and VO(IV) (**9**–**12**) complexes are monometallic, even by using the template method, probably due to their low solubility so that they precipitate immediately in the reaction medium.

Representative examples of the preparation of thio-Schiff bases $H_4L_a$ and $H_2L_b$ of complexes **1** and **12**, respectively, are illustrated and the other complexes were synthesized in the same manner.



#### 4.4.1. *Synthesis of complex $[Co_2(L_a)(H_2O)_4]$ (**1**)*

A solution of 4,6-bis((*E*)-1-(2-mercaptophenylimino)ethyl)benzene-1,3-diol, $H_4L_a$, ligand (0.45 g, 1.102 mmol) in ethanol (30 ml) was added gradually to a solution of $Co(NO_3)_2{\cdot}6H_2O$ (0.641 g, 1.101 mmol) in the same solvent (20 ml) in the molar ratio 1:2 (ligand:metal). The solutions were stirred for 30 min and heated to reflux for 3 h. The solid complexes were precipitated and filtered off, washed with ethanol then diethyl ether and finally air-dried. Yellow precipitate is formed. The complex is air-stable in the solid state and soluble in DMF. The yield was 0.66 g, (60.66%) and the melting point was higher than 250°C.

#### 4.4.2. *Synthesis of complex $[Ru(L_b)(Cl)]{\cdot}2H_2O$ (**12**)*

A solution of 2-((*E*)-1-(6-((*E*)-1-(2-mercaptophenylimino)ethyl)pyridine-2-yl)ethylideneamino) benzenthiol, $H_2L_b$, ligand (0.45 g, 1.102 mmol) in ethanol (30 ml) was added gradually to a solution of the $RuCl_3{\cdot}3H_2O$ (0.621 g, 1.191 mmol) in the same solvent (30 ml) in the molar ratio 1:2, (1 $H_2L_b$:2 metal). The solutions were stirred for 30 min and heated to reflux for 3 h. The solid complexes were precipitated and filtered off, washed with ethanol then diethyl ether and finally air-dried. Black precipitate was formed, giving products of the formula $[Ru(L_b)(Cl)]{\cdot}2H_2O$ (**3**). The complex is air-stable in the solid state and soluble in DMF. The yield was 0.72 g, (67.79%) and the melting point was higher than 250°C. The template method failed in an attempt to afford the expected molar ratio 1:2 (1 $H_2L_b$:2 metal).

### 4.5. *The antimicrobial experiment*

*In vitro* biological screening of the synthesized ligands and complexes were carried out against the phytopathagenic bacteria (*Azotobacter and Rhizobium*) and fungi (*Aspergillus niger* and *Fusarium oxysporium*) by the well diffusion method (*55*). The antimicrobial studies have been carried out at the Faculty of Agriculture, Department of Plant Pathology, Al-Azhar University.

## References


(1) Soliman, A.A.; Linert, W. *Monatsh. Chem*. **2007,** *138*, 175–189.
(2) Sönmez, M.; Bayram, M.R.; Çelebi, M. *J. Coord. Chem*. **2009,** *62*, 2728–2735.
(3) Andrews, A.A.; Langler, R.F. *J. Sulfur Chem.* **2009,** *30*, 137–144.
(4) Harisadhan, G.; Soumya, S.; Abdur, R.A.; Bhisma, K.P. *J. Sulfur Chem.* **2010,** *31*, 1–11.
(5) Chohan, Z.H.; Kausar, S. *J. Met. Based Drugs* **2000,** *7*, 17–22.
(6) Akl, M.A.; Ismail, D.S.; El-Asmy, A.A. *Microchem. J*. **2006,** *83*, 61–69.
(7) Chandra, S.; Lokesh, K.; Sangeetika, G. *Spectrochim. Acta Part A* **2005,** *62*, 453–460.
(8) Singh, P.; Das, S.; Dhakarey, R. *E. J. Chem*. **2009,** *6*, 99–105.
(9) El-Asmy, A.A; Hussanian, M.M; Abdel-Rhman, M.H. *J. Sulfur Chem.* **2010,** *31*, 141–151.
(10) Dhar, S.; Senapati, D.; Das, P.K.; Chattopadhyay, P.; Nethaji, M.; Chakravarty, A.R. *J. Am. Chem. Soc.* **2003,** *125*, 12118–12124.
(11) Wu, J.Z.; Yuan, L. *J. Inorg. Biochem.* **2004,** *98*, 41–45.
(12) McCarthy, P.J.; Hovey, R.J.; Veno, K.; Martell, A.E. *J. Am. Chem. Soc*. **1955,** *77*, 5820–5924.
(13) Panchal, P.K.; Pansuriya, P.B.; Patel, M.N. *J. Enzyme Inhib. Med. Chem.* **2006,** *21*, 453–458.
(14) Christensen, A.; Jensen, H.S.; Mckee, V.; Mckenzie, C.J.; Munch, M. *J. Inorg. Chem.* **1997,** *36*, 6080–6085.
(15) Bernd, G. *Angew. Chem. Int. Ed. Engl*. **1977,** *16*, 125–136.
(16) Athappan, P.; Rajagopal, G. *Transit. Met. Chem*. **1997,** *22*, 167–171.
(17) Yilmaz, I.; Temel, H.; Alp, H. *Polyhedron* **2008,** *27*, 125–132.
(18) Temel, H.; Alp, H.; Ihan, S.; Ziyadanogullari, B.; Yilmaz, I. *Monatsh. Chem.* **2007,** *138*, 1199–1209.
(19) Raman, N.; Kulandaisamy, A.; Thangarja, C.; Jeyasubramanian, K. *Transit. Met. Chem.* **2003,** *28*, 29–36.
(20) Koley, M.K.; Sivasubramanian, S.C.; Varghese, B.M.; Periakaruppan, T.; Koley, A.P. *Inorg. Chim. Acta.* **2008,** *361*, 1485–1495.
(21) Akbar, A.M.; Mohamed, N.; Rina, S.; Ray, J.B.; Jeffrey, C.B. *Polyhedron* **1998,** *17*, 3955–3961.
(22) Prabakaran, R.; Zgeetha, A.; Thilagavathi, M.; Karvembu, R.; Krishnan, V.; Bertagnolli, H.; Natarajan, K. *J. Inorg Biochem*. **2004,** *98*, 1023–1031.
(23) Akbar, A.M.; Teoh, S.G. *J. Inorg. Nucl. Chem.* **1978,** *40*, 451–548.
(24) Pereira, E.; Gomes, L.R.; Low, J.N.; de Castro, B. *Polyhedron* **2007,** *26*, 335–343.
(25) Bellamy, L.J. *The Infrared Spectra of the Complex Molecules*, 2nd ed.; Wiley Interscience: New York, 1970.
(26) Wang, B.; Ma, H.Z.; Shi, Q.Z. *Inorg. Chem. Commun*. **2001,** *4*, 409–412.
(27) Nakamoto, K. *Infrared and Raman Spectra at Inorganic and Coordination Components*, 3rd ed.; New York: John Wiley and Sons, 1986.
(28) Abu-Hussen, A.A.A.; Linert, W. *J. Spectrochim. Acta Part A* **2009,** *74*, 214–223.
(29) Temel, H.; Ilhan, S.; Sekerci, M.; Ziyadanogullari, R. *Spectrosc. Lett.* **2002,** *35*, 219–228.
(30) Ferraro, J.R. *Low Frequency Vibrations of Inorganic and Coordination Compounds*, 2nd ed.; John Wiley: New York, 1971.
(31) Salih, I.; Hamdi, T.; Ismail, Y.; Ahmet, K. *Transit. Met. Chem.* **2007,** *32*, 344–349.
(32) Silverstone, R.M.; Bassler, C.G.; Morrill, T.C. *Spectrometric Identification of Organic Compounds*; John Wiley: New York, 1974.
(33) Cotton, F.A.; Wilkinson, G. *Advanced Inorganic Chemistry, A Comprehensive Text*, 4th ed.; John Wiley and Sons: New York, 1986.
(34) Dutta, R.L.; Syamal, A. *Elements of Magnetochemistry*; East West Press: New Delhi, 1993.
(35) Gerloch, M.; Manning, M.R. *Inorg. Chem.* **1981,** *20*, 1051–1056.
(36) Geary, W. *J. Coord. Chem*. **1971,** *7*, 18–122.
(37) Lever, A.B.P. *Inorganic Electronic Spectroscopy*, 2nd ed.; Elsevier: Amsterdam, 1984.
(38) Abu-Hussen, A.A.; El-Metwally, N.M.; Saad, I.M.; El-Asmy, A.A. *J. Coord. Chem*. **2005,** *58*, 1735–1749.
(39) Anacona, J.R.; Marquez, V.E. *Transit. Met. Chem*. **2008,** *33*, 579–583.
(40) El-Metwally, N.M.; El-Shazly, R.M.; Gabr, I.M.; El-Asmy, A.A. *Spectrochim. Acta Part A* **2005,** *61*, 1113–1119.
(41) Balasbramanian, S.; Krishnan, C.N. *Polyhedron* **1986,** *5*, 669–679.
(42) Speier, G.; Csihony, J.; Whalen, A.M.; Pierpont, C.G. *Inorg. Chem.* **1999,** *35*, 3519–3524.
(43) Kilveson, D. *J. Chem. Phys. B* **1997,** *101*, 8631–8634.
(44) Hathaway, B.J.; Billing, D.E. *Coord. Chem. Rev.* **1970,** *5*, 143–207.
(45) Bencini, A.; Gattechi, D. *EPR of Exchange Coupled System*; Springer-Verlag: Berlin, 1990.
(46) Zhang-lin, Y.; Forissier, M.; Vedrine, J.C.; Volta. J.C. *J. Catal*. **1994,** *145*, 267–280.
(47) El-Metwally, N.M.; Abou-Hussen, A.A.; Gaber, I.M.; El-Asmy, A.A. *Transit. Met. Chem*. **2006,** *31*, 71–78.

(48) Williams, D.H.; Fleming, I. *Spectroscopic Methods in Organic Chemistry*; McGraw-Hill: London, 1989.
(49) Dodd, J.W.; Tonge, K.H. *Thermal Methods; Analytical Chemistry by Open Learning*; John Wiley and Sons: New York, 1987.
(50) Abo-Hussein, A.A.; El-Kholy, S.S.; El-Sabee, M. *J. Coord. Chem*. **2004,** *57*, 1027–1036.
(51) El-Metwally, N.M.; El-Asmy, A.A.; Abou-Hussen, A.A. *Int. J. Pure Appl. Chem.* **2006,** *1*, 75–81.
(52) Vogel, A.I. *Textbook of Quantitative Inorganic Analysis*, 4th ed.; Longman: London, 1978.
(53) Mabbs, F.E.; Machin, D.I. *Magnetism and Transition Metal Complexes*; Chapman and Hall: London, 1973.
(54) Emara, A.A.A.; Abu-Hussen, A.A.A. *Spectrochim. Acta Part A* **2006,** *64*, 1010–1024.
(55) Pelczar, M.J.; Chan, E.C.S.; Krieg, N.R. *Microbiology*, 5th ed.; McGraw-Hill: New York, 1998.